UNIVERSIDAD
NACIONAL
DE COLOMBIA

Integrated Interpretation of Eocene-Palaeocene Rocks in Potwar Basin, Pakistan: Implications for Petroleum Generation

Syed Bilawal Ali Shah*

Department of Geology, University of Malaya,
Kuala Lumpur 50603, Malaysia.
Email: bilawalshah22@siswa.um.edu.my

ABSTRACT

This study demonstrates how an integrated geochemical and petrophysical analysis can be used to evaluate the petroleum generation potential of source and reservoir rocks. The Eocene and Palaeocene sequences of the Potwar Basin, located in the upper Indus Basin of Pakistan, were analyzed. Well logs and Schlumberger log interpretation charts were used for the petrophysical analysis of the Chorgali Formation's reservoir potential. Geochemical methods were applied to 34 well-cutting Sakesar and Patala formations samples. Results from Vitrinite Reflectance (VR) (%Ro) and Tmax data suggest that both formations have reached the peak of their oil generation window. The Sakesar Formation has a mean TOC of 1.88 wt. % and HI values of 375 mg HC/g TOC. The Patala Formation has a mean TOC of 3.33 wt.% in well A and HI values ranging from 2.4 to 369 mg HC/g TOC in well B, with a mean TOC of 3.52 wt%. Both formations have mixed Type II/III kerogen. The findings indicate that both the Sakesar and Patala formations possess good oil/gas-generation potential and may act as source rocks in the Potwar Basin. Petrophysical analysis of the Chorgali Formation shows an average porosity of 10.32%, water saturation of 36.14%, and hydrocarbon saturation of 63.85%. This indicates that the Chorgali Formation has an average to good reservoir potential. The research findings will aid exploration and production companies in the Fimkassar Oilfield.

Interpretación integrada de rocas del Eoceno y el Paleoceno en la cuenca Potwar, Pakistán: implicaciones para la generación petrolífera

RESUMEN

Este estudio muestra como un análisis geoquímico y petrofísico integrado se puede usar para evaluar el potencial de generación petrolífera de las rocas fuente y reservorio. Con este fin se analizaron las secuencias del Eoceno y del Paleoceno de la cuenca Potwar, localizada en la cuenca superior de Indus, en Pakistán. Se utilizaron los registros de pozo y los gráficos de interpretación de registros de Schlumberger para el análisis petrofísico del potencial reservorio de la Formación Chorgali. Se aplicaron métodos geoquímicos a 34 láminas cortadas de pozo en las formaciones Sakesar y Patala. Los resultados de reflectancia de la vitrinita (VR) (%Ro) y los datos Tmax sugieren que ambas formaciones han alcanzado el pico de su período de generación petrolera. La formación Sakesar tiene una media TOC de 1.88 wt. % y valores HI de 375 mg HC/g TOC. La formación Patala tiene una media TOC de 3.33 wt. % en el pozo A y valores HI que van de 2.4 a 369 mg HC/g TOC en el pozo B, con una media TOC de 3.52 wt. %. Ambas formaciones tienen mezclados tipos II y III de querógeno. Los hallazgos indican que ambas formaciones tienen un buen potencial de generación de petróleo y gas y pueden actuar como las rocas fuentes de la cuenca Potwar. Los análisis petrofísicos de la formación Chorgali muestran un promedio de porosidad de 10.32 %, saturación de agua de 36.14 % y saturación de hidrocarburos de 63.85 %. Esto indica que la Formación Corgali tiene un buen potencial como reservorio. Los resultados del trabajo ayudarán en la exploración y producción de las compañías en el campo petrolero de Fimkassar.

1. Introduction

The Potwar Basin is a productive oil and gas-producing basin in Pakistan. Several researchers have provided information on the sources of hydrocarbons in the basin, including Imtaiz et al. (2017), Fazeelat et al. (2010), Ihsan et al. (2022), and Shah (2022). Hydrocarbon traps in the Potwar Basin are primarily structurally controlled, although there are also stratigraphic traps (Asif et al., 2011; He et al., 2023; Yasin et al., 2021; Zhou et al., 2022). In this study, sediments from two wells in the Fimkassar oilfield and well logs have been analyzed (Fig. 1). According to various studies, the primary source of hydrocarbons in the Potwar Basin is the Patala Formation. These researchers include Asif et al. (2011), Fazeelat et al. (2010), Fazeelat et al. (2009), Shah et al. (2022), Shah and Shah (2021), Shah (2022), and Yasin et al. (2021). The sediments from two wells of the Fimkassar oilfield, which are of the Eocene and Palaeocene ages, have been studied (Fig. 1).

A study by Fazeelat et al. (2011) and Shah (2022) found that shallow marine sediments in the Potwar Basin contain organic-rich matter, necessitating an evaluation and interpretation of the source and reservoir rock characteristics of the Chorgali, Patala, and Sakesar formations in the basin (Table 1).

The novel contribution of this research is the thorough study of well cutting samples and well logs to assess source rock generation potential, thermal maturity, identification of kerogen type, and petrophysical properties. Additionally, this research combines two different methods to evaluate the horizon for potential prospects and two essential properties of the petroleum system, namely source and reservoir rock properties. This is the unique aspect of this research work. Previous studies by researchers such as Ihasn et al. (2022),

Table 1. Qualitative description of reservoirs porosity set by Rider's (1986) and Shah et al. (2021).

Qualitatively Evaluation of Porosity	
Qualitative description	Average Porosity
Negligible	0-5
Poor	5-10
Good	10-20
Very Good	20-30
Excellent	>30

Nazir et al. (2014), Shah et al. (2021), Fazeelat et al. (2010), Shah (2017), Nazir et al. (2015), H et al. (2021), and Masood et al. (2017) focused on different formations and used various techniques to evaluate them, including modelling the structure with faults for salt diapirs and studying specific formations like Sakesar, Tobra, and Khewra. However, there is a lack of information regarding the interpretation of all three formations' source and reservoir rock properties, which makes this study necessary and crucial.

The Fimkassar oilfield is located in the Potwar Basin (Fig. 1). The findings of this study will reveal the source and reservoir rock generation potential, kerogen type, thermal maturity of the rocks as source rocks, and the presence of possible hydrocarbon prospects. The research outcomes will directly benefit future hydrocarbon exploration by oil and gas companies. This research will
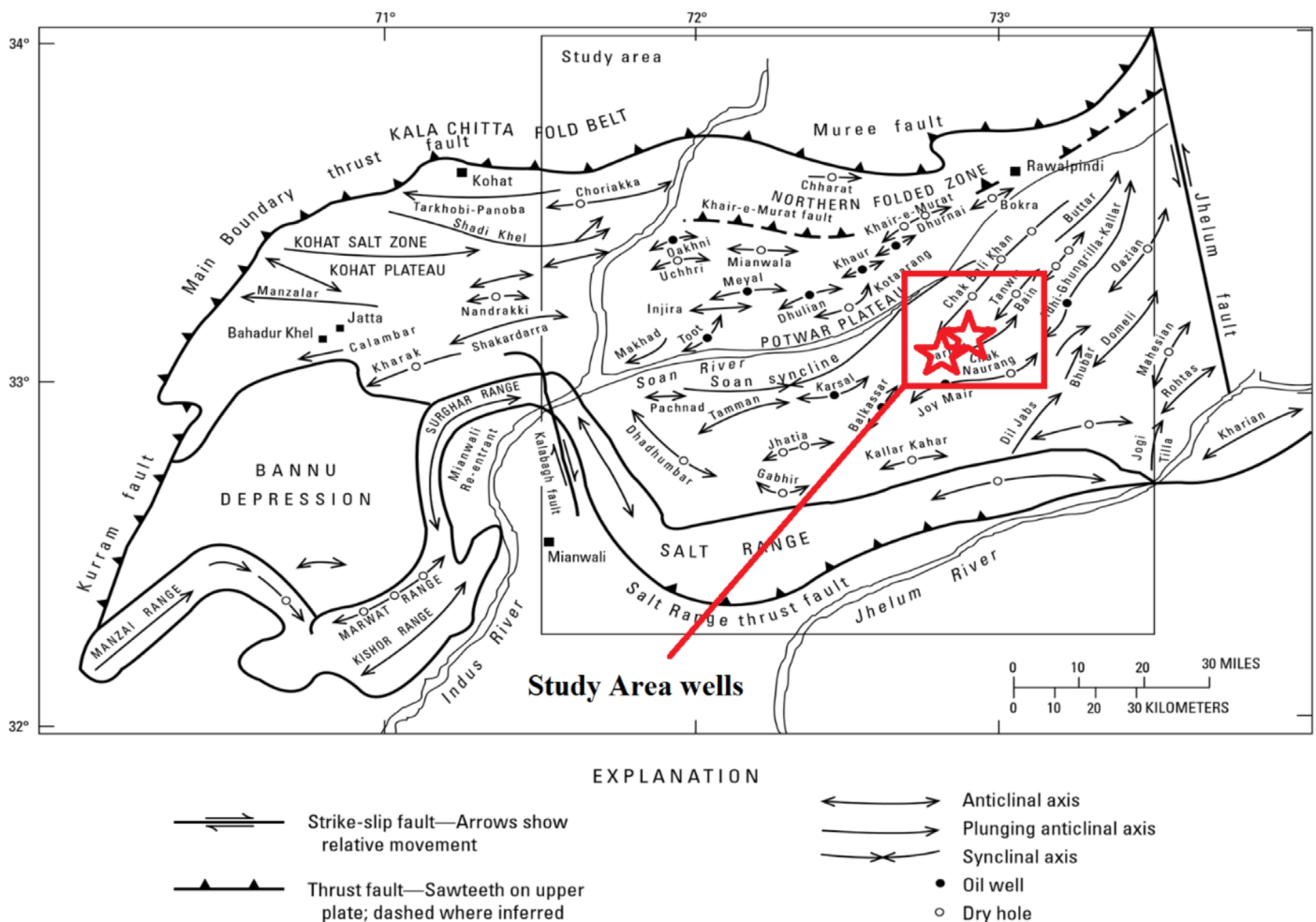
Figure 1. Map showing location of wells and major tectonic structures of Potwar Basin (after Shami and Baig, 2002; Zahid et al., 2014; Shah and Abdullah, 2016; Shah and Abdullah, 2017; Shah et al., 2019).

contribute valuable information to the existing body of knowledge, aiding in the understanding of various source and reservoir properties and the petroleum potential for future hydrocarbon exploration and production.

2. Geological setting

The Potwar Basin exhibits several major characteristics, including inner and outer folded zones, a platform, and a foredeep comprising depressions (Kadri, 1995; Kazmi and Jan, 1997; Liu et al., 2023; Nazir and Fazeelat, 2017; Zhan et al., 2022). The study area specifically refers to the Fimkassar oilfield.

The Potwar Basin is geographically divided into two sections by the Indus and Jhelum rivers in the east and west, respectively. It is bordered by the Salt Range in the south and the Kalachitta-Margalla hill ranges in the north (Cheng and Fu, 2022; Liu et al., 2023; Shah and Abdullah, 2017; Yin et al., 2023). The basin is characterized by east-west complex and tight folds, which are inverted in the south and affected by steep-angle faults. The northern portion of the basin experiences more extensive deformation (Aadil et al., 2014; Kazmi & Abbassi, 2002; Kazmi & Jan, 1997; Riaz, 2022; Shah, 2009; Shah, 2022). In contrast, the eastern part of the basin exhibits an abrupt change in strike towards the northeast, with structures consisting of large synclines and anticlines tightly folded. The western part of the basin contains several gentle and broad east-west folds (Fu et al., 2022; Shah, 2022; Yin et al., 2023; Zahid et al., 2012; Zhang et al., 2022).

2.1 An overview of the Potwar Basin's source and reservoir rocks

The Potwar Basin has several known source rocks, including the Sakesar, Hangu, Patala, and Lockhart formations (Shah, 2022; Xu et al., 2022; Zheng et al., 2023) (Table 2). The reservoir rocks found in the Potwar Basin include alluvial and shoreface Cambrian sandstones, Miocene alluvial sandstones, Jurassic and Permian continental sandstones, Paleogene shelf carbonates, and Miocene alluvial sandstones (Aadil et al., 2014; Kazmi & Abbassi, 2002; Liu et al., 2023; Peng et al., 2022). Oil and gas have been explored from reservoir

Table 2. General stratigraphy of Potwar Basin (Modified after Fazeelat et al., 2010; Shah and Abdullah, 2017).

AGE / EPOCH		LITHOLOGY	FORMATION	LITHOLOGY DESCRIPTION
Neogene	Pliocene		Nagri Chinji	Sandstone, sandstone and clay
	Miocene Oligocene		Kamlial Murree	Sandstone, sandstone, limestone
Oligocene		Unconformity		
Paleogene	Eocene		Chorgali Sakesar	Limestone, limestone
	Paleocene		Patala Lockhart Hangu	Shale, limestone, sandstone
Mesozoic & Late Permian		Unconformity		
Jurassic			Datta	Sandstone, Shale
Permian	Early Permian		Chhidru Wargal Amb Sardhai Warcha Dandot Tobra	Sandstone, limestone, limestone, siltstone, interbeds of sandstone, shale interbeds of sandstone, sandstone and conglomerate.
Carboniferous to Ordovician		Unconformity		
Cambrian to Precambrian	Cambrian		Baghanwala Jutana Kussak Khewra	Shale, dolomite, sandstone and siltstone, Shale interbeds of dolomite and siltstone
	Infra-Cambrian		Salt Range	Marl, claystone and siltstone, Salt
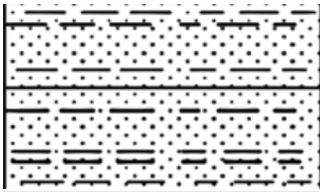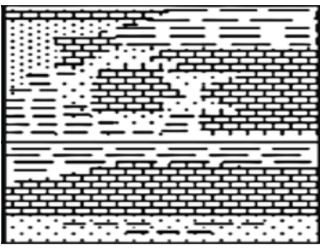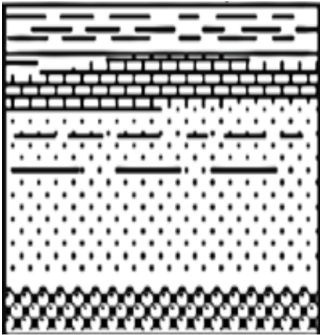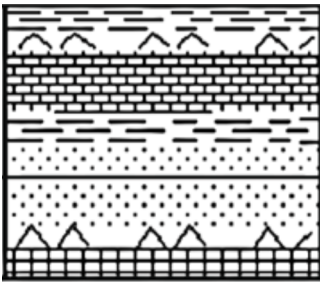
rocks such as Tobra, Wargal, Amb, Cambrian Khewra, Jutana, Kussak, Jurassic Dutta, Khairabad, Lockhart, Nammal, Sakesar, Margalla Limestone, Chorgali, Bhadrar, and Murree (Zahid et al., 2012). The discovered oilfields in the Potwar Basin are found in either pop-up structures, faulted anticlines, or fault-block traps (Shah, 2022; Xu et al., 2022; Zheng et al., 2023; Zhou et al., 2022).

3. Materials and methods

Thirty-four well cutting samples were obtained from the Fimkassar oilfield in the Potwar Basin, collected from Palaeocene and Eocene sequences. Well A provided samples at intervals of 4-15 m, while well B provided samples at intervals of 5-6 m. Detailed information about the samples can be found in Table 5.

Reservoir rock characteristics were determined using various logs, including density, neutron, gamma ray, resistivity, and spontaneous potential logs. The reservoir properties were qualitatively described based on criteria from Rider (1986) and Shah and Shah (2021). This study specifically utilized well logs from Well A to investigate the reservoir potential of the Nammal Formation. Reservoir rock characteristics were evaluated using methods proposed by Shah (2022), Shah (2021), and Hartmann and Beaumont (1999). Furthermore, calculations were performed to determine hydrocarbon saturation, porosity, water saturation, and formation water resistivity.

3.1 Organic petrographic analyses

The analysed samples were dried and crushed to approximately 1-2mm in size. The sediments were then embedded in polyester resin (Serifix) with a hardener, allowing the resin to set. Once set, the samples were flattened on a diamond lap and polished using various grades of silicon carbide paper, lubricated with isopropyl alcohol. Subsequently, the samples were further polished with increasingly finer alumina powder (5/20, 3/50, and gamma) to achieve a highly reflective surface. Vitrinite reflectance measurements were conducted using a Leica CTR6000M microscope equipped with Diskus Fossil software. Calibration was performed using a leuko-sapphire standard (0.589% Ro). Considering the availability and distribution of vitrinite particles, between 15-50 measurements were obtained. The measurements were taken using an oil immersion X50 objective lens under white light.

3.2 Organic geochemical analysis

The well cutting samples were initially crushed to obtain fine particles smaller than 200 mesh. The total organic carbon (TOC) content was then measured using LECO elemental analysers, specifically the CS-125 model. Pyrolysis analysis was performed using the Rock-Eval VI equipment. Approximately 100mg of crushed samples were subjected to pyrolysis in a helium atmosphere, heated to 600°C. The pyrolysis process provided three crucial parameters: S1, representing the amount of whole free petroleum; S2, indicating the quantity of hydrocarbons generated

during thermal cracking; and Tmax, the temperature at which the maximum hydrocarbon generation occurs (Shah, 2023; Shah and Shah, 2021). The hydrogen index and production yield were also calculated as other significant factors.

3.3 Well log analysis

The well logs in the LAS file format were used on the interactive petrophysics software package to establish reservoir properties. Details of the properties are available in Table 3.

The procedure for obtaining various parameters from the well logs is described in the section below:

The log track parameters that were directly read included:
1. Formation depth (ft.)
2. Neutron porosity (NPHI; 0.45 to -0.15 scale)
3. Bulk resistivity of the formation (LLD; 0 – 2000ohm.m scale)
4. Spontaneous potential (SP; 0 – 100mv scale)
5. Bulk density of formation (RHOB; 1.95 –2.95 scale)

Volume of shale (Vsh):

The volume of shale was calculated using GR logs. Vsh was calculated using the equation below. (Rider, 2002; Shah, 2023; Shah et al., 2022):

$$GR = (GR\_log-GR\_min/GR\_max-GR\_min)$$

Porosity calculation:

Sonic log was used to determine the porosity by using the following equation:

$$\Phi s = \Delta Tlog–\Delta tma/\Delta Tf–\Delta tma$$

Where,

$\Delta Tlog$ = Sonic transit time

ΔTf = Travel transit time of interstitial fluid (189 μs/ft. for fresh mud and 185 μs/ft. Salt mud)

Δtma = Travel transit time of matrix material (47.6 μs/ft. for limestone)

Effective porosity:

The permeable zone of the formation is determined by calculating effective porosity. Following equation was used to calculate effective porosity (Rider, 2002; Shah et al., 2023; Xu et al., 2022; Zhang et al., 2022):

$$\phi e = \phi t*(1-Vsh)$$

Whereas: ϕe= Effective porosity ϕt = Total porosity

Vsh = volume of shale

Table 3. Petrophysical analysis ifferent parameters calculated for well logs analysis.

Depth (ft)	Temp	RHOB	ΦD	SP	Φ (N.D)	Rt (LLD)	Rwe	Rw	Sw	SH	Lithology
7944	151.6	2.61	0.13	-27	0.12	330	0.39	0.67	36%	64%	Limestone
7969	152.2	2.62	0.10	-12	0.14	310	0.51	0.80	39%	61%	Limestone
7994	152.7	2.64	0.12	-28	0.11	160	0.62	0.61	37%	63%	Limestone
8019	153.1	2.63	0.09	-33	0.09	950	0.56	0.47	35%	65%	Limestone
8044	153.5	2.61	0.11	-25	0.13	1390	0.27	0.32	38%	62%	Limestone
8069	154.4	2.67	0.08	-32	0.10	1680	0.62	0.44	32%	68%	Limestone
8094	154.6	2.66	0.11	-35	0.13	480	0.35	0.35	36%	64%	Limestone

Hydrocarbon Saturation (SH)

Spontaneous potential (SP) method (Figure 2-3b) was used for the determination of hydrocarbons at the zone of interest. The graphs and equations used together in the following process:

1. Formation temp was calculated using Figure 2 and the following equation: Tf = Ts + Df (BHT-Ts/TD)
2. Rmf and Rm were corrected (Fig. 3a).
3. Sp values were read from logs directly.
4. Rmf/Rwe ratio was calculated (Fig 3b).
5. The Rwe was calculated by Rmf/Rwe ratio.
6. Rwe= Rmfeq/(Rmfeq/Rwe)

7. Water saturation was calculated using Archie's equation:

$$S_w = \sqrt{\frac{R_w}{\phi^m * R_t}}$$

8. Hydrocarbon saturation was calculated using equation: SH=1-Sw

After measuring the resistivity values of the mud filtrate, they were converted to equivalent mud filtrate resistivity values using the equation in Figure 2. To obtain the equivalent water resistivity, the equivalent mud filtrate resistivity values were used according to step 6. Subsequently, the equivalent
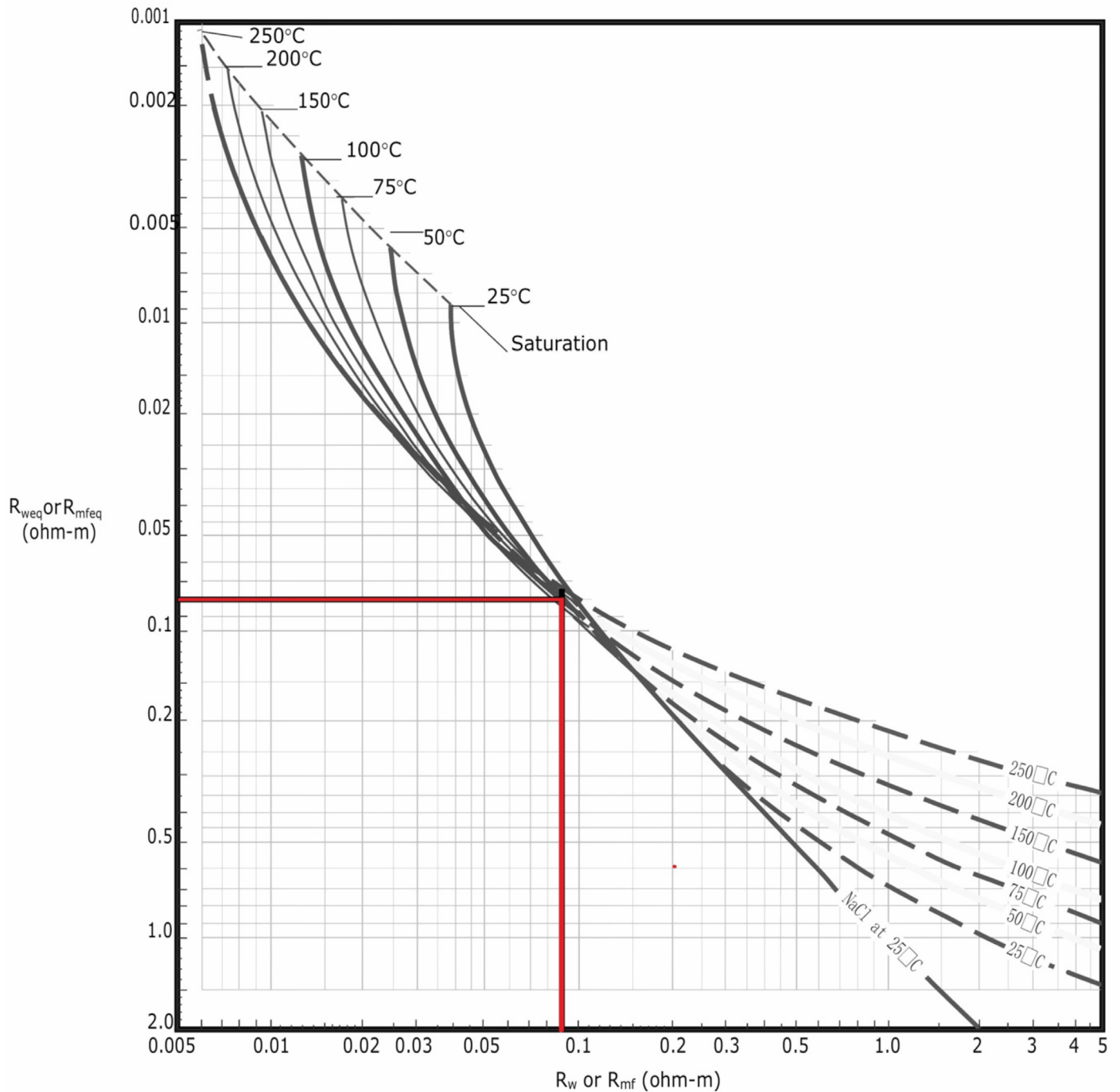
Figure 2. Shows the determination of R_w using Schlumberger chart by determining R_{we}.

Conversion approximated by $R_2 = R_1[(T_1+6.77)/(T_2+6.77)]°F$ or $R_2 = R_1[(T_1+21.5)/(T_2+21.5)]°C$
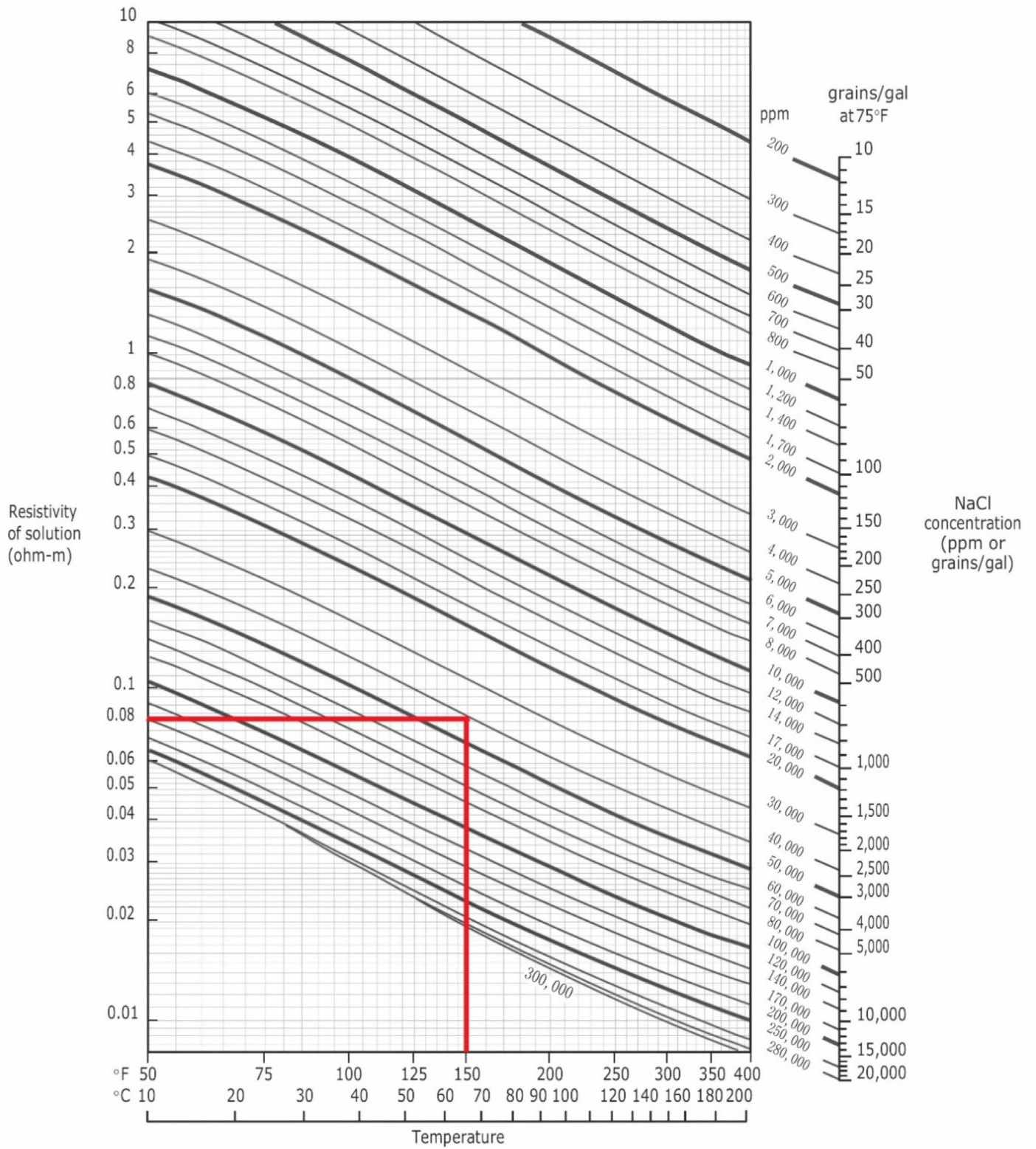
Figure 3. (a) According to temperature Rmf and Rwe correction (Schlumberger, 1977).
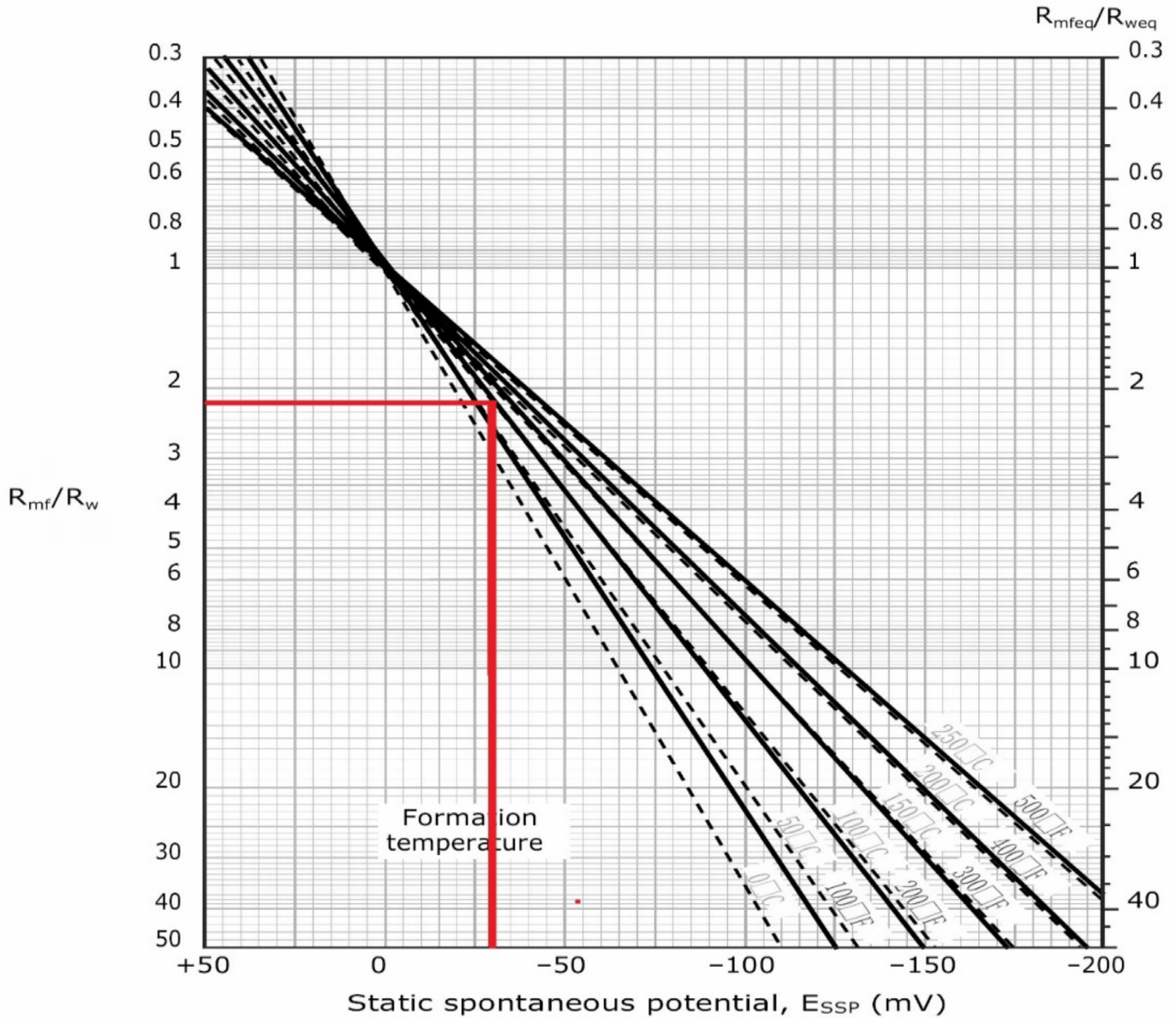
Figure 3. (b) Determination of Rmf/Rwe based on Self-Potential (Schlumberger, 1977).

water resistivity was converted to water resistivity, which was then used to determine water saturation using Archie's equation.

The log header's mud filtrate resistivity was determined at surface temperature. To determine the mud filtrate resistivity at formation temperature, it must be corrected to formation temperature for each value at a certain depth, and this correction was made using the equation presented in Figure 3a.

4. Results and discussion

4.1 Total Organic Carbon and Pyrolysis

Typically, the total organic carbon (TOC) content is used to indicate the richness of rocks, with a TOC value of 1.0% considered necessary for a clastic rock to qualify as a source rock, as stated by Hunt (1996) and Shah (2023). Sediments from the Patala Formation in both wells exhibited higher TOC contents, with mean values ranging from 2.70 wt% to 2.88 wt% in well A and 2.48 wt% to 2.98 wt% in well B, respectively. Sediments from the Sakesar Formation had an average TOC content of 1.72 wt% and ranged from 1.56 wt%

to 1.88 wt%. Based on the sample analysis, the majority of samples showed good to very good TOC content.

The parameter S2, produced during pyrolysis, is the most useful for estimating the hydrocarbon generative potential (Dang et al., 2023; Peters and Cassa, 1994; Tissot and Welte, 1984; Wu et al., 2022). According to Bordenave et al. (1993) and Shah and Abdullah (2017), a good petroleum generation capacity requires a minimum of 5 mg HC/g S2. In general, the Sakesar Formation exhibited hydrocarbon yields (S2) ranging from 3.76 mg/g to 5.78 mg/g, while the Patala Formation in well A showed hydrocarbon yields ranging from 7.88 mg/g to 9.65 mg/g, and the Patala Formation in well B showed hydrocarbon yields ranging from 5.87 mg/g to 8.66 mg/g. The Sakesar Formation displayed fair to good petroleum generating potential, whereas sediments from the Patala Formations in both wells A and B showed good petroleum generating potential, as indicated by the S2 versus TOC cross plots (Fig. 4 and 5).

The migration index (S1/TOC) can be used to differentiate between indigenous and migrated petroleum (Shah, 2022; Tissot and Welte, 1984). The S1 versus TOC plot in this study demonstrated that all samples from the Sakesar Formation and Patala Formation (wells A and B) were indigenous (Fig. 6).
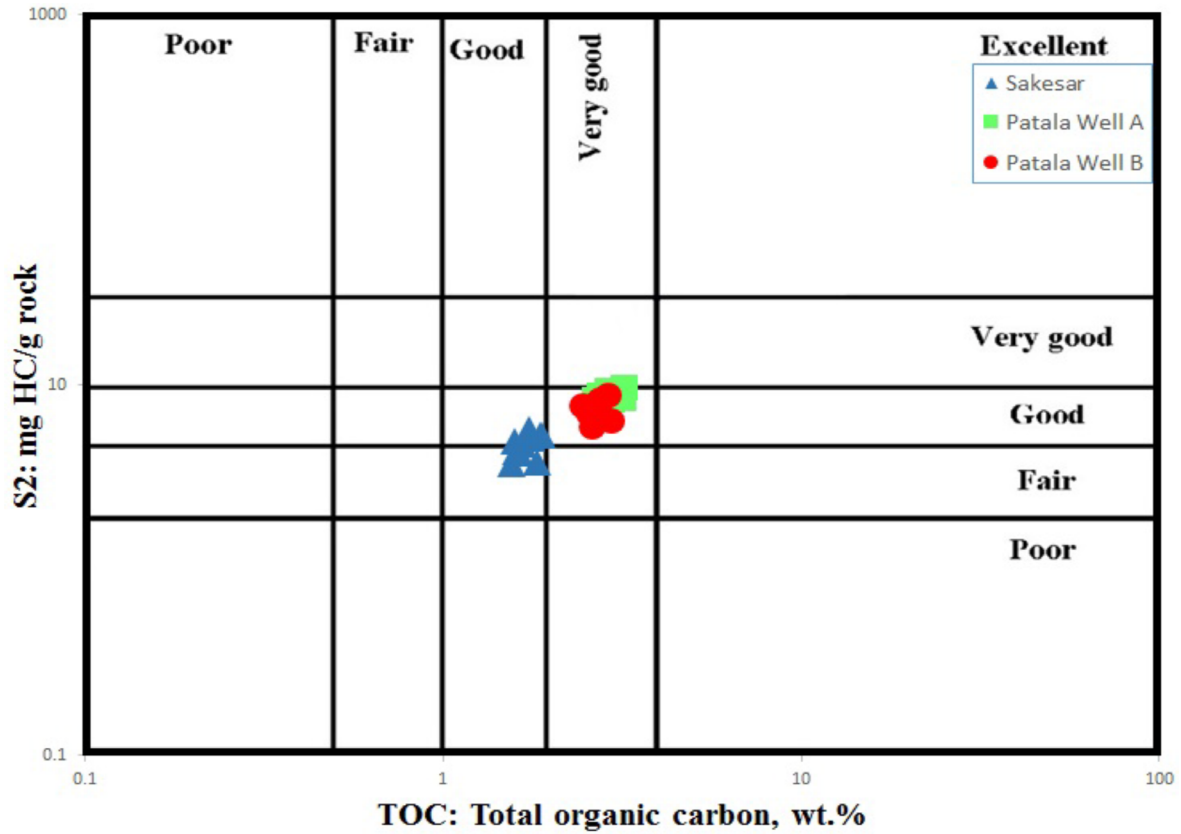
Figure 4. Pyrolysis S2 versus total organic carbon (TOC) plot, showing generative source rock potential for the analyzed samples (Peter and Cassa, 1994).
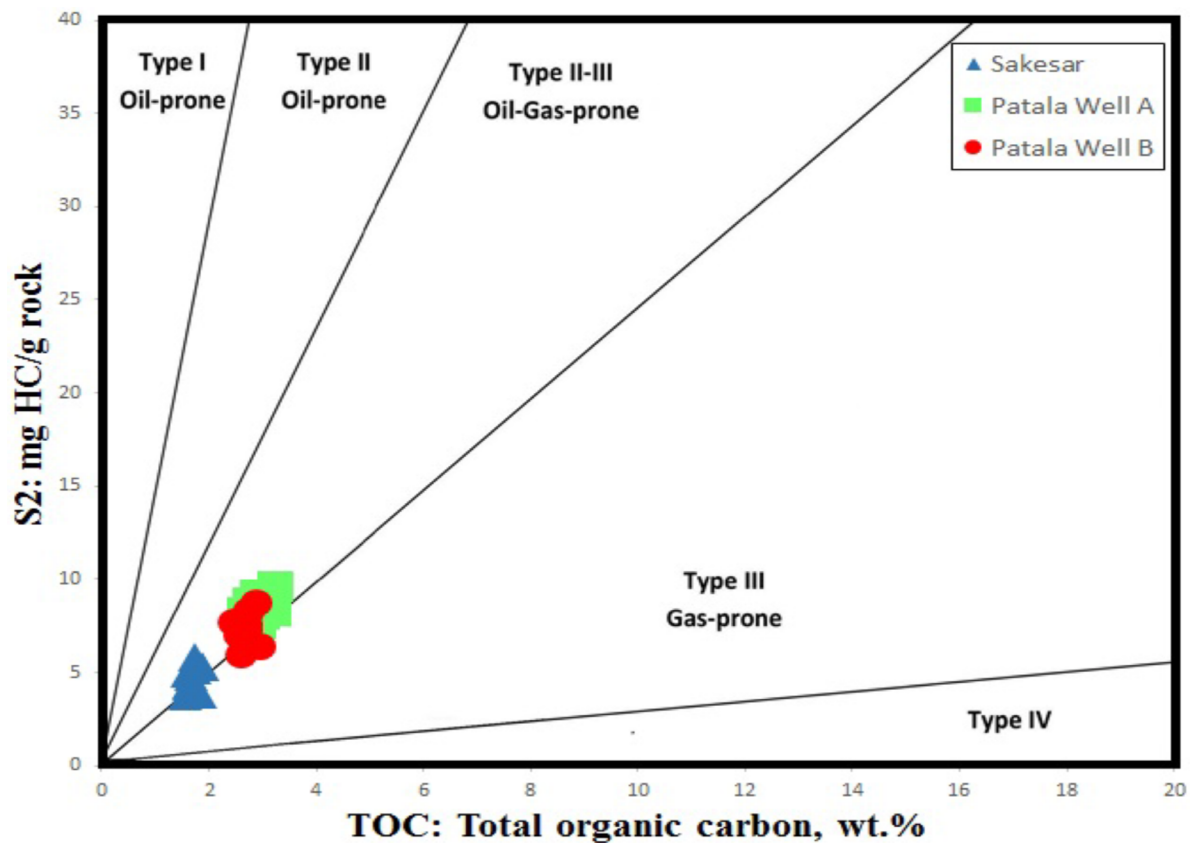
Figure 5. Pyrolysis S2 versus total organic carbon (TOC) plot, showing the type of kerogen for the analyzed samples (Peter and Cassa, 1994).
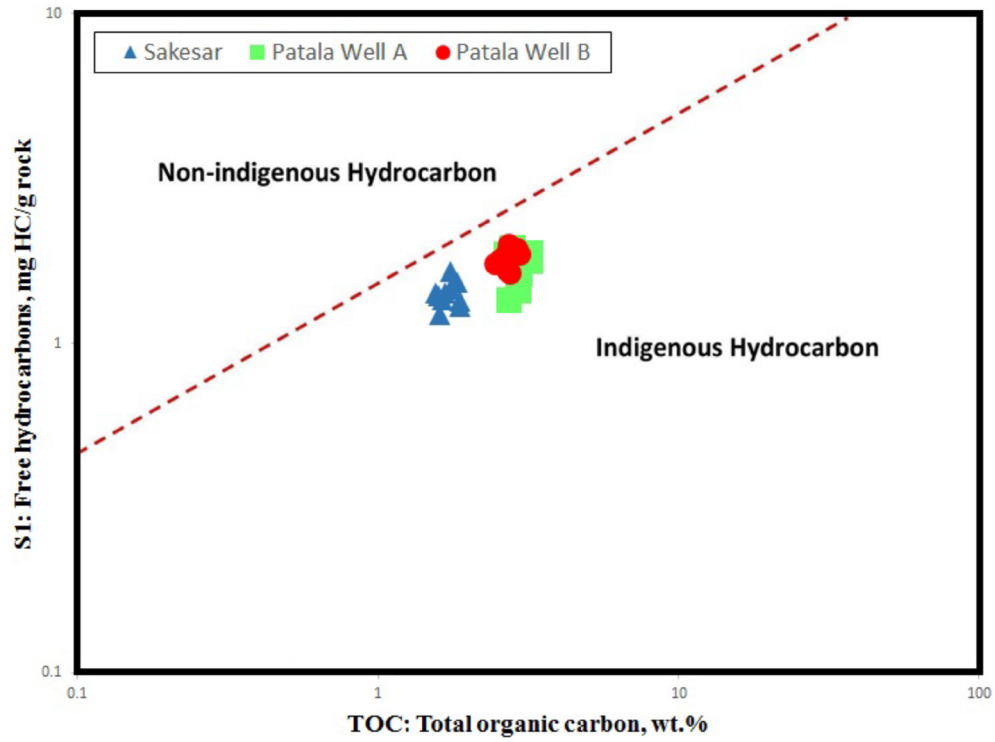
Figure 6. Cross plot of pyrolysis S1 versus total organic carbon (TOC) for identifying the migration index of the studied samples (Hunt, 1996).
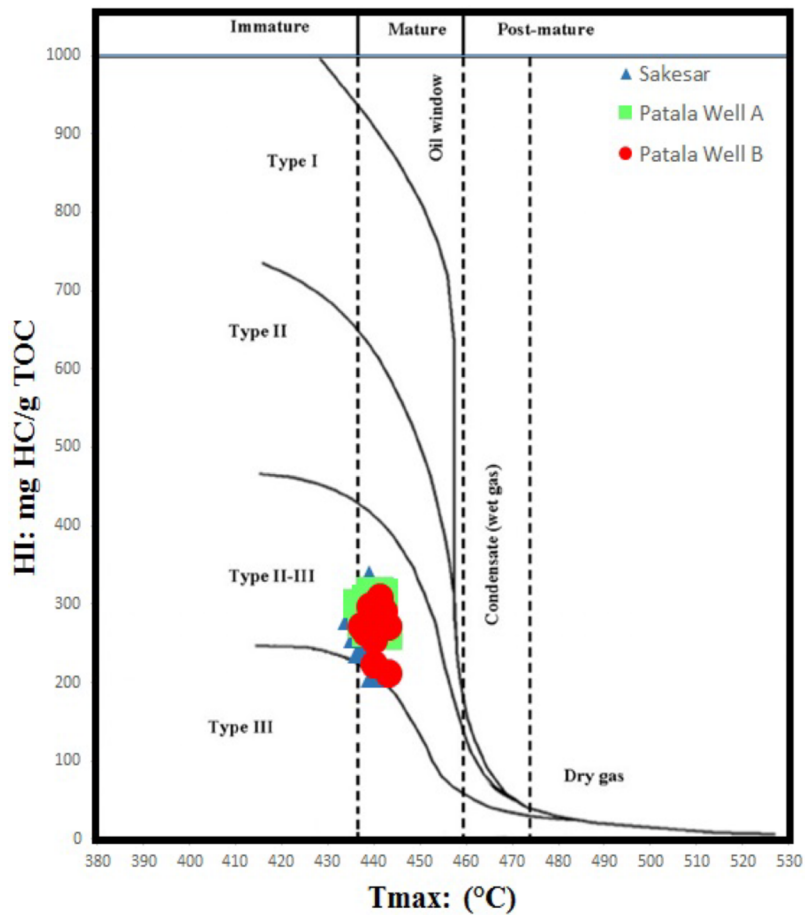
Figure 7. The Pyrolysis HI versus Tmax plot shows kerogen type for the analyzed samples (Mukhopadhyay et al., 1995).
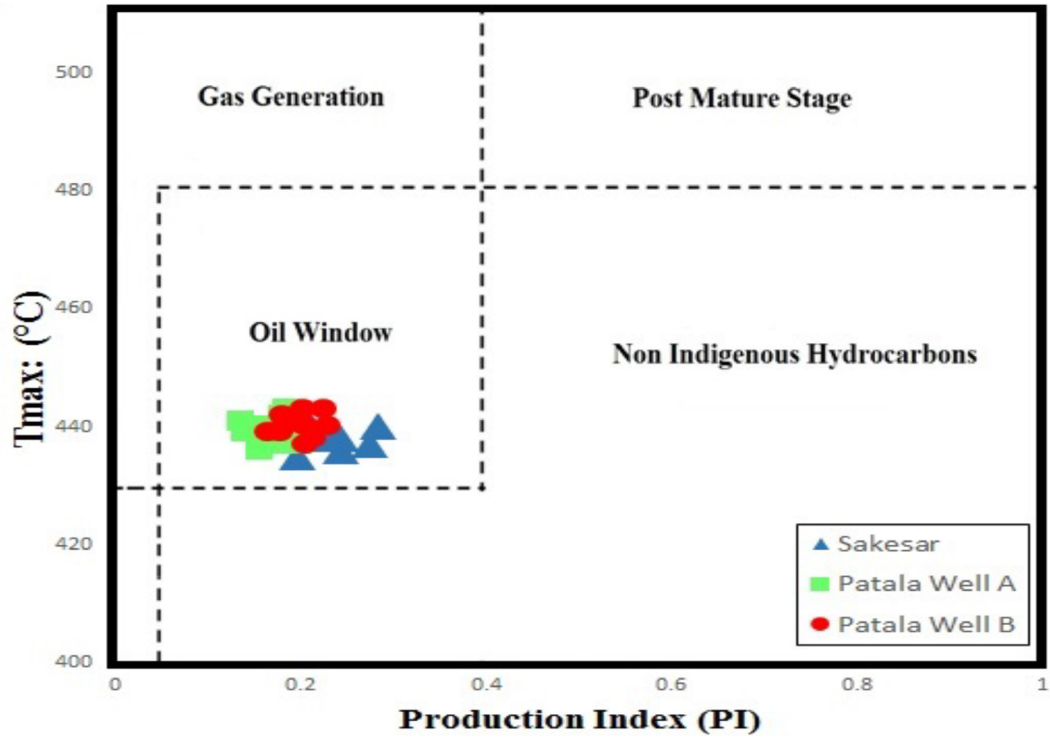
Figure 8. Plot of Tmax versus production index (PI), showing the maturation and nature of the hydrocarbon products of the analyzed samples (Shah, 2023).
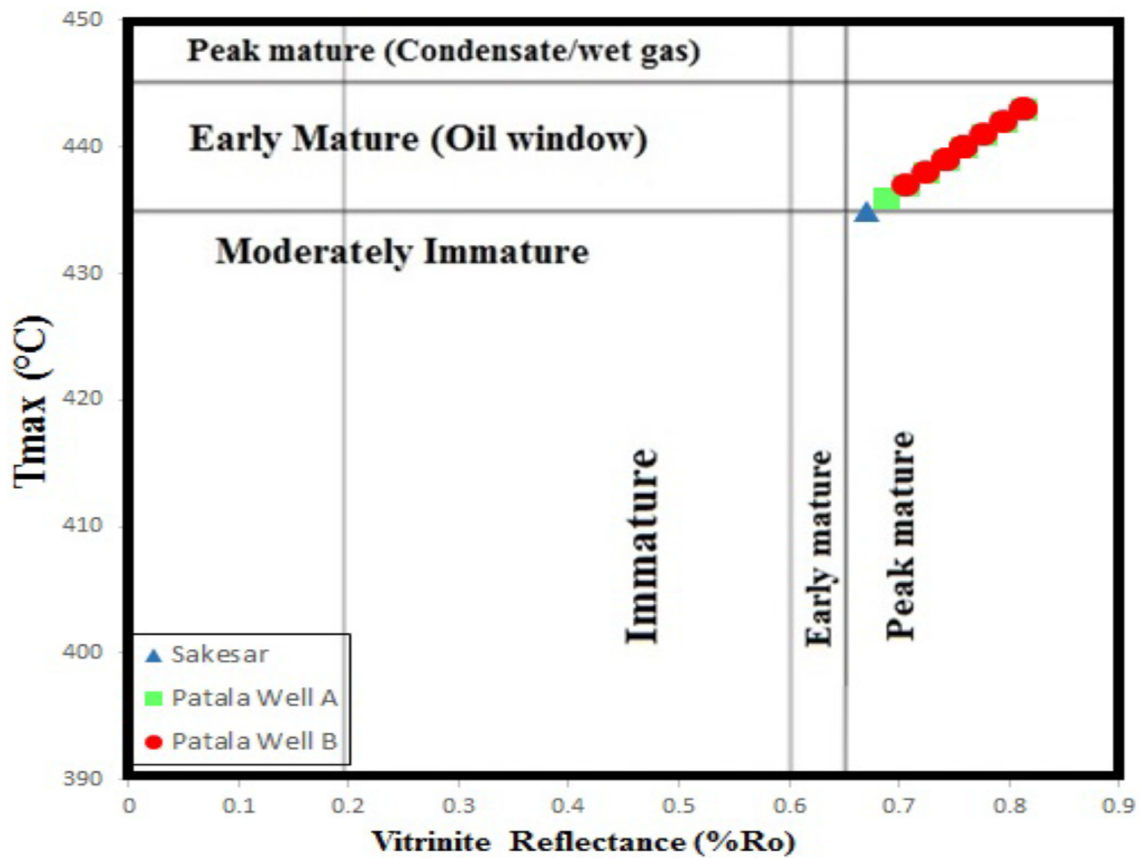
Figure 9. Plot of Tmax versus vitrinite reflectance (Ro) showing the maturity levels (Shah, 2022).

Table 4. Results of analyzed samples of Sakesar and Patala formations presented as summary.

Formation Name and No of samples	Depth (m)	Petroleum Potential				Maturity of sample	Quality of OM	Kerogen Type	Source rock generative potential
		TOC wt. %	S1	S2	S3	Tmax °C	HI		
Sakesar (10)	2938-3076	1.56-1.88	1.23-1.65	3.76-5.78	0.39-0.87	435-442	211-332	Mixed Type II/III and Type III	Fair to good
Patala Well A (13)	3092-3136	2.67-3.21	1.36-1.96	7.88-9.65	0.57-0.88	436-443	262-317		Good
Patala Well B (11)	3055-3106	2.48-2.98	1.63-1.98	5.36-8.66	0.78-0.97	437-443	213-308		

Table 5. Bulk geochemical results of all analysed samples in detail including all test results (VR, TOC and Rock-Eval data).

Formation	Depth (m)	TOC %	Tmax °C	S1	S2	S3	PI	HI	OI	S2/S3	VR
SAKESAR	2938	1.63	436	1.36	4.26	0.47	0.24	261	28.8	9.064	0.69
SAKESAR	2953	1.56	437	1.42	3.76	0.39	0.27	241	25	9.641	0.71
SAKESAR	2969	1.88	435	1.3	5.34	0.75	0.2	284	39.9	7.12	0.67
SAKESAR	2984	1.61	439	1.23	4.36	0.45	0.22	271	28	9.689	0.74
SAKESAR	2999	1.58	438	1.4	4.97	0.78	0.22	315	49.4	6.372	0.72
SAKESAR	3015	1.74	439	1.47	5.78	0.87	0.2	332	50	6.644	0.74
SAKESAR	3030	1.87	442	1.35	5.34	0.54	0.2	286	28.9	9.889	0.8
SAKESAR	3045	1.67	440	1.42	4.78	0.65	0.23	286	38.9	7.354	0.76
SAKESAR	3061	1.75	438	1.65	5.13	0.78	0.24	293	44.6	6.577	0.72
SAKESAR	3076	1.83	440	1.53	3.86	0.73	0.28	211	39.9	5.288	0.76
PATALA	3092	2.81	437	1.96	7.88	0.63	0.2	280	22.4	12.51	0.71
PATALA	3096	2.67	438	1.87	8.23	0.77	0.19	308	28.8	10.69	0.72
PATALA	3099	2.78	442	1.94	8.78	0.73	0.18	316	26.3	12.03	0.8
PATALA	3103	2.71	439	1.36	8.26	0.82	0.14	305	30.3	10.07	0.74
PATALA	3107	2.91	441	1.45	9.21	0.63	0.14	316	21.6	14.62	0.78
PATALA	3110	2.97	437	1.78	8.2	0.57	0.18	276	19.2	14.39	0.71
PATALA	3114	2.86	438	1.88	7.89	0.78	0.19	276	27.3	10.12	0.72
PATALA	3118	3.21	436	1.79	9.65	0.67	0.16	301	20.9	14.4	0.69
PATALA	3121	2.95	440	1.63	8.64	0.88	0.16	293	29.8	9.818	0.76
PATALA	3125	3.2	443	1.89	8.37	0.83	0.18	262	25.9	10.08	0.81
PATALA	3129	2.89	438	1.77	7.63	0.79	0.19	264	27.3	9.658	0.72
PATALA	3132	2.76	439	1.83	8.75	0.86	0.17	317	31.2	10.17	0.74
PATALA	3136	2.82	440	1.75	8.45	0.72	0.17	300	25.5	11.74	0.76
Well B											
PATALA	3055	2.74	438	1.98	7.23	0.78	0.21	264	28.5	9.269	0.72
PATALA	3060	2.57	437	1.79	6.98	0.95	0.2	272	37	7.347	0.71
PATALA	3065	2.63	440	1.75	5.87	0.89	0.23	223	33.8	6.596	0.76
PATALA	3070	2.98	443	1.86	5.36	0.78	0.26	180	26.2	6.872	0.81
PATALA	3075	2.48	441	1.74	7.65	0.95	0.19	308	38.3	8.053	0.78
PATALA	3081	2.72	439	1.65	7.58	0.83	0.18	279	30.5	9.133	0.74
PATALA	3086	2.65	440	1.73	6.74	0.96	0.2	254	36.2	7.021	0.76
PATALA	3091	2.68	443	1.85	7.28	0.82	0.2	272	30.6	8.878	0.81
PATALA	3096	2.77	439	1.63	8.25	0.93	0.16	298	33.6	8.871	0.74
PATALA	3101	2.91	440	1.93	8.66	0.78	0.18	298	26.8	11.1	0.76
PATALA	3106	2.67	442	1.71	7.78	0.97	0.18	291	36.3	8.021	0.8

4.2 Kerogen Type

The hydrogen index (HI) was utilized to assess the kerogen types in the formations, which is considered the most important index for this purpose (Peters, 1986; Tissot and Welte, 1984). HI values for the Sakesar Formation ranged from 211 mg HC/g TOC to 332 mg HC/g TOC, while the Patala Formation exhibited HI values ranging from 262 to 317, and well B showed HI values ranging from 213 to 308. To classify the kerogen type, HI versus Tmax plots were constructed, revealing that the sediments of all formations primarily consist of mixed Type-II/III kerogen. The kerogen type identified through S2 versus TOC plots also aligned with the interpretation of the HI versus Tmax plot (Fig. 4 and 7).

Samples from both wells A and B in the Patala Formation exhibited high HI values of 213 to 317 mg HC/g TOC, while samples from the Sakesar Formation also displayed high HI values of 211 to 332 mg HC/g TOC, indicating their potential as oil/gas-prone source rocks (Fig. 4, 5).

4.3 Thermal maturity

For thermal maturity assessment, parameters including Tmax values, vitrinite reflectance (%Ro), and Production Index (PI) were used. Oil with vitrinite reflectance values ranging from 0.6% to 1.3%Ro is considered thermogenic oil (Bordenave, 1993; Tissot and Welte, 1984). Tmax levels exhibit a wide range of variation. According to Espitalié et al. (1977) and Shah et al. (2023), Tmax values between 430 and 455 °C correspond to kerogen Types I and II, while values between 435 and 465 °C correspond to Type III.

All formations showed measured vitrinite reflectance (%Ro) values ranging from 0.67% to 0.81% (Figure 8). As shown in Table 4, the vitrinite reflectance values for the Sakesar Formation sediments ranged from 0.67% to 0.8% Ro and corresponded to temperatures between 435 and 442 °C, indicating the peak of oil production and early maturity within the oil window (Fig. 9). In the case of the Patala Formation, samples from well A exhibited vitrinite reflectance values ranging from 0.69% to 0.81% Ro, with Tmax values between 436 and 443 °C, while samples from well B exhibited vitrinite reflectance values ranging from 0.71% to 0.81% Ro, with Tmax values varying between 437 and 443 °C (Table 4 and 5). These values suggest early maturity within the oil window and the peak of oil generation (Fig. 9).

For organic matter maturity assessment, if PI values are less than 0.05, the samples may be considered immature and may have produced little to no hydrocarbons. PI values between 0.05 and 0.10 indicate very limited oil production and a potential entry into the wet gas zone. PI readings exceeding 1.0 suggest that the kerogen's capacity to produce hydrocarbons may have been depleted.

Sediments from the Sakesar Formation exhibited PI values ranging from 0.2 to 0.28, indicating early to peak maturity, which aligns with the Tmax and vitrinite reflectance (%Ro) measurements (Fig. 8). Meanwhile, samples from the Patala Formation predominantly displayed PI values ranging from 0.14 to 0.26, indicating early to peak maturity within the oil window, and were consistent with the Tmax and %Ro data (Fig. 8).

4.4 Reservoir potential

The reservoir parameters determined from the petrophysical analysis were used for the quantitative interpretation of the reservoir. The estimated petrophysical characteristics of the Chorgali Formation are shown in Table 3. The average porosity ranged between 8-14%, indicating poor to moderate reservoir potential. According to Rider (1986) and Shah and Shah (2021) criteria, the average water saturation was 36.14%, and the hydrocarbon saturation was 63.85%, indicating average to good hydrocarbon potential (Table 1).

5. Concluding remarks

Following is a summary of the key findings from the investigation of the Chorgali, Patala, and Sakesar formations sediments using geochemical and petrophysical analysis:

The source rock sediments showed that the Sakesar Formation has fair to good generative ability, with TOC > 1.5 wt. % (ranging from 1.56-1.88 wt.

%), and possesses mixed Type II/III Kerogen. The Patala Formation has good to very good generative potential, with TOC > 2.4 wt. % (ranging from 2.48-3.21 wt. % in both wells). Both formation sediments lie in the maturity oil/gas window zone, as indicated by both S2 vs TOC and HI vs Tmax plots. Therefore, it could be expected that both formations may have generated oil and gas in the Fimkassar Oilfield subsurface.

Petrophysical analysis of the Chorgali Formation encountered in well A indicates average reservoir qualities and an average potential for the production of hydrocarbons.

References

Aadil, N., & Sohail, G. M. (2014). 3D geological modelling of Punjab Platform, Middle Indus Basin Pakistan through Integration of wireline Logs and seismic data. *Journal of the Geological Society of India*, 83(2), 211-217. doi:10.1007/s12594-014-0033-2.

Asif, M., Fazeelat, T., & Grice, K. (2011). Petroleum geochemistry of the Potwar Basin, Pakistan: 1. Oil-oil correlation using biomarkers, δ13C and δD. *Organic Geochemistry*, 42(10), 1226-1240. DOI:10.1016/j.orggeochem.2011.08.003.

Asif, M., Nazir, A., Fazeelat, T., Grice, K., Nasir, S., & Saleem, A. (2011). Applications of polycyclic aromatic hydrocarbons to assess the source and thermal maturity of the crude oils from the Lower Indus Basin, Pakistan. *Petroleum Science and Technology*, 29(21), 2234-2246. DOI:10.1080/10916461003699226.

Bordenave, M. L., Espitalié, J., Leplat, P. O. J. L., Oudin, J. L., & Vandenbroucke, M. (1993). Screening techniques for source rock evaluation. *Applied Petroleum Geochemistry*, 217-278.

Cheng, Y., & Fu, L. (2022). Nonlinear seismic inversion by physics-informed Caianiello convolutional neural networks for overpressure prediction of source rocks in the offshore Xihu depression, East China. *Journal of Petroleum Science and Engineering*, 215, 110654. DOI:10.1016/j.petrol.2022.110654.

Bordenave, M. L. (1993). *Applied Petroleum Geochemistry*. Editions Technip, Paris.

Cheema, M. R., Raza, S. M., & Ahmad, H. (1977). Stratigraphy of Pakistan. *Memoirs of the Geological Survey of Pakistan, Quetta* 12(1), 56–98.

Dang, P., Cui, J., Liu, Q., & Li, Y. (2023). Influence of source uncertainty on stochastic ground motion simulation: a case study of the 2022 Mw 6.6 Luding, China, earthquake. *Stochastic Environmental Research and Risk Assessment*. DOI:10.1007/s00477-023-02427-y.

Espitalié, J., Laporte, J. L., Madec, M., Marquis, F., Leplat, P., Paulet, J., & Boutefeu, A. (1977). Methode rapide de caractérisation des roches mères, de leur potentiel pétrolier et de leur degré d'évolution. *Revue de L'Institut Français du Pétrole*, 32(1), 23-42. DOI:10.2516/ogst:1977002.

Fazeelat, T., Jalees, M. I., & Bianchi, T. S. (2010). Source rock potential of Eocene, Paleocene and Jurassic deposits in the subsurface of the Potwar Basin, northern Pakistan. *Journal of Petroleum Geology*, 33(1), 87-96. DOI:10.1111/j.1747-5457.2010.00465.x.

Fazeelat, T., Asif, M., Jalees, M. I., Saleem, A., Nazir, A., Saleem, H., Nasir, S., & Nadeem, S. (2011). Source correlation between biodegraded oil seeps and a commercial crude oil from the Punjab Basin. *Journal of Petroleum Science and Engineering*, 77(1), 1-9. DOI:10.1016/j.petrol.2011.01.003.

Fazeelat, T., Asif, M., Saleem, A., Nazir, A., Zulfiqar, M. A., Naseer, S., & Nadeem, S. (2009). Geochemical investigation of crude oils from different. *Journal of the Chemical Society of Pakistan*, 31(6), 863-870.

Fu, Q., Si, L., Liu, J., Shi, H., & Li, Y. (2022). Design and experimental study of a polarization imaging optical system for oil spills on sea surfaces. *Applied Optics*, 61(21), 6330-6338. DOI:10.1364/AO.456305.

Hartmann, D. J., & Beaumont, E. A. (1999). Treatise of Petroleum Geology/Handbook of Petroleum Geology: Exploring for Oil and Gas Traps. Chapter 9: Predicting Reservoir System Quality and Performance, 9-1.

He, H., Tuo, S., Lei, K., & Gao, A. (2023). Assessing quality tourism development in China: an analysis based on the degree of mismatch and its influencing factors. *Environment, Development and Sustainability*. DOI:10.1007/s10668-023-03107-1.

He, M., Dong, J., Jin, Z., Liu, C., Xiao, J., Zhang, F., & Deng, L. (2021). Pedogenic processes in loess-paleosol sediments: Clues from Li isotopes of leachate in Luochuan loess. *Geochimica et Cosmochimica Acta*, 299, 151-162. DOI:10.1016/j.gca.2021.02.021.

Hunt, J. M., Philp, R. P., & Kvenvolden, K. A. (2002). Early developments in petroleum geochemistry. *Organic geochemistry*, 33(9), 1025-1052. https://doi.org/10.1016/S0146-6380(02)00056-6

Ihsan, S., Fazeelat, T., Imtiaz, F., & Nazir, A. (2022). Geochemical characteristics and hydrocarbon potential of Cretaceous Upper Shale Unit, Lower Indus Basin, Pakistan. *Petroleum Science and Technology*, 40(3), 257-269. DOI:10.1080/10916466.2021.1993913.

Imtiaz, F., Fazeelat, T., Nazir, A., & Ihsan, S. (2017). Geochemical characterization of sediment samples of Sembar Formation from three different wells of Southern Indus Basin. *Petroleum Science and Technology*, 35(7), 633-640. DOI:10.1080/10916466.2016.1274757.

Kadri, I. B. (1995). *Petroleum Geology of Pakistan*. Pakistan Petroleum Limited.

Kazmi, A. H., & Jan, M. Q. (1997). *Geology and Tectonics of Pakistan*. Graphic Publishers.

Kazmi, A. H., & Abbasi, I. A. (2008). *Stratigraphy and Historical Geology of Pakistan* (1st. ed., Vol. 1). Department & National Centre of Excellence in Geology Press, Peshawar.

Liu, H., Ding, F., Li, J., Meng, X., Liu, C., & Fang, H. (2023). Improved Detection of Buried Elongated Targets by Dual-Polarization GPR. *IEEE Geoscience and Remote Sensing Letters*, 20. DOI:10.1109/LGRS.2023.3243908.

Liu, Z., Xu, J., Liu, M., Yin, Z., Liu, X., Yin, L., & Zheng, W. (2023). Remote sensing and geostatistics in urban water-resource monitoring: a review. *Marine and Freshwater Research*, 74(10). DOI:10.1071/MF22167.

Liu, Z., Feng, J., & Uden, L. (2023). From technology opportunities to ideas generation via cross-cutting patent analysis: Application of generative topographic mapping and link prediction. *Technological Forecasting and Social Change*, 192, 122565. DOI:10.1016/j.techfore.2023.122565.

Masood, F., Ahmad, Z., & Khan, M. S. (2017). Moderate Interpretation with Attribute Analysis and 3d Visualization for Deeper Prospects of Balkassar Field, Central Potwar, Upper Indus Basin, Pakistan. *International Journal of Geosciences*, 8(05), 678. DOI:10.4236/ijg.2017.85037.

Mukhopadhyay, P. K., Wade, J. A., & Kruge, M. A. (1995). Organic facies and maturation of Cretaceous/Jurassic rocks and possible oil-source rock correlation based on pyrolysis of asphaltenes, Scotian basin, Canada. *Organic Geochemistry*, 22, 85-104. DOI:10.1016/0146-6380(95)90010-1.

Nazir, A., & Fazeelat, T. (2014). Petroleum geochemistry of Lower Indus Basin, Pakistan: I. Geochemical interpretation and origin of crude oils. *Journal of Petroleum Science and Engineering*, 122, 173-179. DOI:10.1016/j.petrol.2014.07.008.

Nazir, A., Fazeelat, T., & Asif, M. (2015). Petroleum geochemistry of lower Indus Basin, Pakistan: II. Oil-oil and oil-source rock correlation. *Petroleum Science and Technology*, 33(12), 1295-1304. DOI:10.1080/10916466.2015.1060502.

Nazir, A., & Fazeelat, T. (2017). Geochemistry of Cretaceous rocks, Pakistan: II. Interpretation of source, depositional environment and lithology of organic matter. *Petroleum Science and Technology*, 35(10), 937-946. DOI:10.1080/10916466.2017.1286509.

Peng, J., Xu, C., Dai, B., Sun, L., Feng, J., & Huang, Q. (2022). Numerical Investigation of Brittleness Effect on Strength and Microcracking Behaviour of Crystalline Rock. *International Journal of Geomechanics*, 22(10), 4022178. DOI:10.1061/(ASCE)GM.1943-5622.0002529.

Peters, K. E. (1986). Guidelines for evaluating petroleum source rock using programmed pyrolysis. *AAPG Bulletin*, 70(3), 318-329. DOI:10.1306/94885688-1704-11D7-8645000102C1865D.

Peters, K. E., & Cassa, M. R. (1994). Applied Source Rock Geochemistry. In: Magoon, L. B., Dow, W. G. (Eds.). *The Petroleum System – From Source to Trap*. American Association of Petroleum Geologists Memoir, Vol. 60, 93-120. AAPG, Tulsa, Oklahoma, USA

Riaz, M. (2022). Subsurface Structural Interpretation of Missa Keswal, Eastern Potwar, Pakistan. *Journal of Earth Sciences and Technology*, 3(2), 17-28.

Rider, M. H. (1986). *The Geological Interpretation of Well Logs*. Rider-French Publications

Schlumberger. (1977). *Charts Schlumberger Log Interpretation*. Schlumberger Limited, New York.

Shah, S. B. A., & Abdullah, W. H. (2016). Petrophysical properties and hydrocarbon potentiality of Balkassar well 7 in Balkassar oilfield, Potwar Plateau, Pakistan. *Bulletin of the Geological Society of Malaysia*, 62, 73-77. DOI:10.7186/bgsm62201610.

Shah, S. B. A., & Abdullah, W. H. (2017). Structural interpretation and hydrocarbon potential of Balkassar oil field, eastern Potwar, Pakistan, using seismic 2D data and petrophysical analysis. *Journal of the Geological Society of India*, 90(3), 323-328. DOI:10.1007/s12594-017-0720-x.

Shah, S. B. A., Abdullah, W. H., & Shuib, M. K. (2019). Petrophysical properties evaluation of Balkassar oilfield, Potwar Plateau, Pakistan: Implication for reservoir characterization. *Himalayan Geology*, 40(1), 50-57.

Shah, S. B. A., & Shah, S. H. A. (2021). Hydrocarbon Generative Potential of Cretaceous and Jurassic Deposits in the Ahmedpur East Oilfield Subsurface, Punjab Platform, Pakistan. *Journal of the Geological Society of India*, 97(8), 923-926. DOI:10.1007/s12594-021-1792-1.

Shah, S. B. A. (2021). Lockhart formation provides source rocks for Potwar Basin. *Oil & Gas Journal*, 119(8), 22-28.

Shah, S. B. A. (2022). Evaluation of organic matter in Sakesar and Patala formations in southern and northern Potwar Basin, Pakistan. *Petroleum Science and Technology*. DOI:10.1080/10916466.2022.2105360.

Shah, S. B. A., Shah, S. H. A., & Jamshed, K. (2023). An integrated palynofacies, geochemical and petrophysical analysis for characterizing mixed organic-rich carbonate and shale rocks in Potwar Basin, Pakistan: Insights for multisource and reservoir rocks evaluation. *Journal of Petroleum Science and Engineering*, 5, 168. doi:10.1016/j.petrol.2022.111236.

Shah, S. B. A. (2023). Evaluation of mixed organic-rich carbonate and shale rocks of Meyal oilfield using an integrated palynofacies, geochemical and petrophysical approaches. *Petroleum Science and Technology*. DOI:10.1080/10916466.2023.2175864.

Shah, S. B. A., Shah, S. H. A., & Nath, Manabendra. (2023). 1-D Basin modelling, 3-D reservoir mapping and source rock generative potential of Balkassar oilfield, Potwar Basin, Pakistan. *Petroleum Science and Technology*. DOI:10.1080/10916466.2023.2175866.

Shah, S. B. A. (2023). Evaluation of mixed organic-rich carbonate and shale rocks of Meyal oilfield using an integrated palynofacies, geochemical and petrophysical approaches. *Petroleum Science and Technology*. DOI:10.1007/s12517-023-11365-6.

Shah, S. B. A. (2022). Investigation of the hydrocarbon generative potential of Eocene, Cretaceous, and Late Triassic age sequences in the Punjab Platform Basin, Pakistan, using geochemical and petrophysical techniques. *Carbonates and Evaporites Journal*. DOI:10.1007/s13146-022-00842-w.

Shah, S. B. A. (2022). Evaluation of organic matter in Sakesar and Patala formations in southern and northern Potwar Basin, Pakistan. *Petroleum Science and Technology*. DOI:10.1080/10916466.2022.2105360.

Shami, B. A., & Baig, M. S. (2002). *Geomodeling for enhancement of hydrocarbon potential of Joya Mair Field (Potwar) Pakistan*. PAPG-SPE Annual Technical Conference, Islamabad (pp. 124-145).

Shah, S. M. I. (2009). Stratigraphy of Pakistan. *Geological Survey of Pakistan*, 22, 25-39.

Tissot, B. P., & Welte, D. H. (1984). *Petroleum Formation and Occurrence* (2nd ed.). Springer, New York.

Wu, M., Ba, Z., & Liang, J. (2022). A procedure for 3D simulation of seismic wave propagation considering source-path-site effects: Theory, verification and application. *Earthquake Engineering & Structural Dynamics,* 51(12), 2925-2955. DOI: 10.1002/eqe.3708.

Xu, L., Cai, M., Dong, S., Yin, S., Xiao, T., Dai, Z., & Reza Soltanian, M. (2022). An upscaling approach to predict mine water inflow from roof sandstone aquifers. *Journal of Hydrology*, 612, 128314. DOI: 10.1016/j.jhydrol.2022.128314.

Xu, Z., Wang, Y., Jiang, S., Fang, C., Liu, L., Wu, K., & Chen, Y. (2022). Impact of input, preservation and dilution on organic matter enrichment in lacustrine rift basin: A case study of lacustrine shale in Dehui Depression of Songliao Basin, NE China. *Marine and Petroleum Geology,* 135, 105386. DOI:10.1016/j.marpetgeo.2021.105386.

Xu, Z., Li, X., Li, J., Xue, Y., Jiang, S., Liu, L., & Sun, Q. (2022). Characteristics of Source Rocks and Genetic Origins of Natural Gas in Deep Formations, Gudian Depression, Songliao Basin, NE China. *ACS Earth and Space Chemistry*, 6(7), 1750-1771. DOI: 10.1021/acsearthspacechem.2c00065.

Yasin, Q., Baklouti, S., Khalid, P., Ali, S. H., Boateng, C. D., & Du, Q. (2021). Evaluation of shale gas reservoirs in complex structural enclosures: A case study from Patala Formation in the Kohat-Potwar Plateau, Pakistan. *Journal of Petroleum Science and Engineering*, 198, 108225. DOI: 10.1016/j.petrol.2020.108225.

Yin, L., Wang, L., Ge, L., Tian, J., Yin, Z., Liu, M., & Zheng, W. (2023). Study on the Thermospheric Density Distribution Pattern during Geomagnetic Activity. *Applied Sciences*, 13(9). DOI:10.3390/app13095564.

Yin, L., Wang, L., Tian, J., Yin, Z., Liu, M., & Zheng, W. (2023). Atmospheric Density Inversion Based on Swarm-C Satellite Accelerometer. *Applied Sciences*, 13(6). DOI: 10.3390/app13063610.

Zahid, M., Khan, A., ur Rashid, M., Saboor, A., & Ahmad, S. (2014). Structural interpretation of Joya Mair oil field, south Potwar, Upper Indus Basin, Pakistan, using 2D seismic data and petrophysical analysis. *Journal of Himalayan Earth Sciences*, 47(1), 73-86.

Zhang, X., Ma, F., Dai, Z., Wang, J., Chen, L., Ling, H., & Soltanian, M. R. (2022). Radionuclide transport in multi-scale fractured rocks: A review. *Journal of Hazardous Materials,* 424(Pt C), 127550. DOI: 10.1016/j.jhazmat.2021.127550.

Zhan, C., Dai, Z., Soltanian, M. R., & de Barros, F. P. J. (2022). Data-worth analysis for heterogeneous subsurface structure identification with a stochastic deep learning framework. *Water Resources Research*, e2022W-e33241W. DOI:10.1029/2022WR033241.

Zhang, K., Wang, Z., Chen, G., Zhang, L., Yang, Y., Yao, C., & Yao, J. (2022). Training effective deep reinforcement learning agents for real-time life-cycle production optimization. *Journal of Petroleum Science and Engineering*, 208, 109766. DOI: 10.1016/j.petrol.2021.109766.

Zheng, Z., Zuo, Y., Wen, H., Li, D., Luo, Y., Zhang, J., & Zeng, J. (2023). Natural gas characteristics and gas-source comparisons of the lower Triassic Feixianguan formation, Eastern Sichuan basin. *Petroleum Science*. DOI:10.1016/j.petsci.2023.02.005.

Zheng, Z., Zuo, Y., Wen, H., Zhang, J., Zhou, G., Xv, L., & Zeng, J. (2022). Natural gas characteristics and gas-source comparisons of the Lower Triassic Jialingjiang Formation, Eastern Sichuan Basin. *Journal of Petroleum Science and Engineering*, 111165. DOI: 10.1016/j.petrol.2022.111165.

Zhou, J., Wang, L., Zhong, X., Yao, T., Qi, J., Wang, Y., & Xue, Y. (2022). Quantifying the major drivers for the expanding lakes in the interior Tibetan Plateau. *Science Bulletin*, 67(5), 474-478. DOI:10.1016/j.scib.2021.11.010.

Zhou, G., Song, B., Liang, P., Xu, J., & Yue, T. (2022). Voids Filling of DEM with Multiattention Generative Adversarial Network Model. *Remote Sensing*, 14(5), 1206. DOI: 10.3390/rs14051206.